Electronic Supplementary Material (ESI) for Journal of Materials Chemistry A.

Electronic Supplementary Material

Preparation multifunctional porous carbon materials through direct laser writing on the phenolic resin film

Junbo Liu, Lijing Zhang, Cheng Yang, and Shengyang Tao*

Department of Chemistry, Dalian University of Technology, Dalian, Liaoning, P. R. China. Email: taosy@dlut.edu.cn;

Supporting Figures and Tables

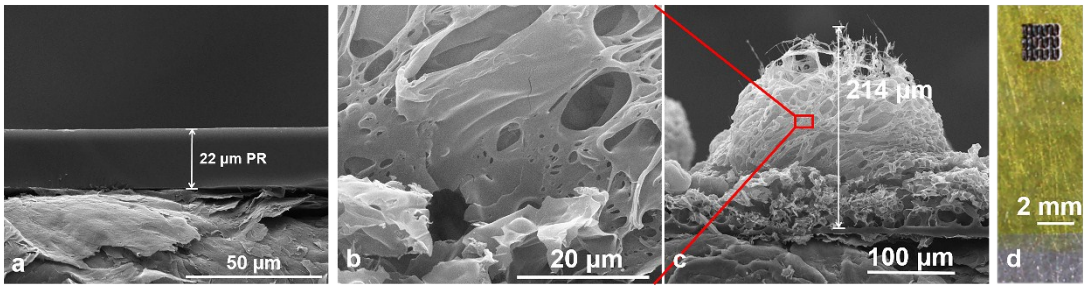

Figure S1. a) Cross-sectional SEM images of the PR film. b) and c) Cross-sectional SEM images of the PCE. d) A photo of PCE.

Finite-element simulation analysis of the temperature of the laser spot:

A laser beam moved on the PR film substrate to produce a PCE. The laser power and the laser scan rate were recorded as P and v, respectively. The surface emissivity of the PR film substrate was ε. The transient temperature of the laser spot could be obtained by finite-element simulation.

The incident heat flux of the laser determined the temperature of the surface of the PR film substrate. In the operating wavelength range of the laser, we assumed that the PR film substrate was opaque and the absorptivity was equal to the emissivity. Therefore, no light penetrated the PR film substrate. The PR film substrate absorbed all the heat generated by the laser. The laser thermal load should be multiplied by ε.

The energy conservation law as follow:

$$\rho C_p \frac{\partial T}{\partial t} + \rho C_p u \cdot \nabla T + \nabla \cdot q = Q + Q_{ted} \quad (1)$$

Where ρ is the density of PR, C_p is the constant pressure heat capacity, T is temperature, t is time. Heat flux q ($W \cdot m^{-2}$) is defined as: $q = -\kappa \nabla T$, here κ ($W \cdot m^{-1} k^{-1}$) is heat conductivity. Heat flux of the surface of the PR film substrate is defined as: $q_0 = \varepsilon \times q$.

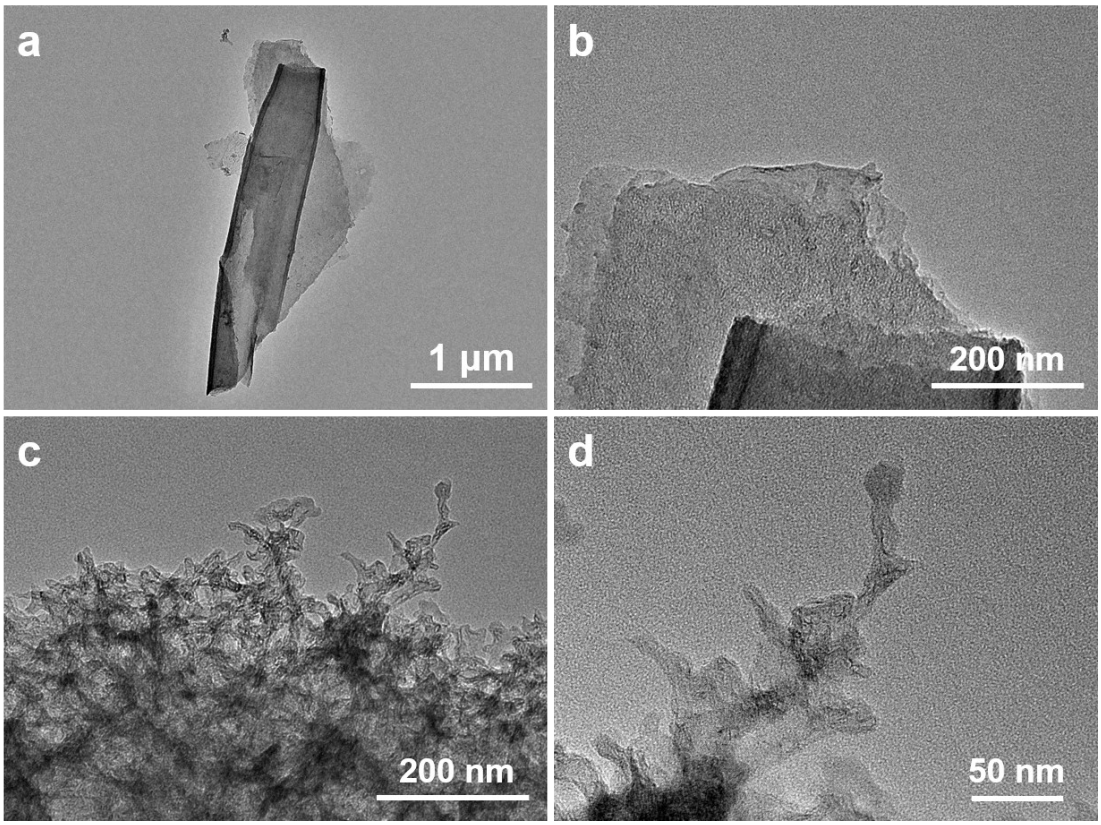

Figure S2. TEM images of PCE.

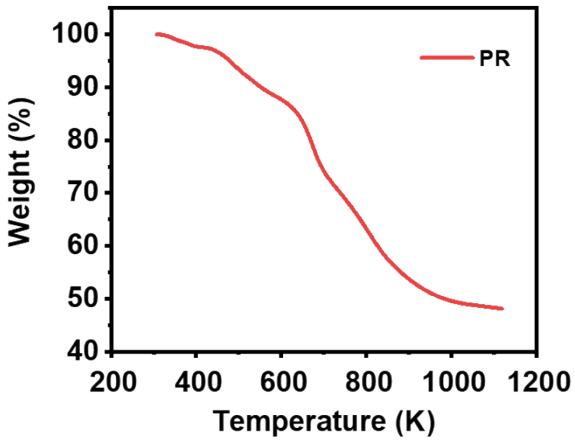

Figure S3. Thermal gravimetric analysis (TGA) of phenolic resin.

Table S1. TGA data of phenolic resin.

Weight (%)	99.99	90.00	50.00	48.58
Temperature (K)	307.47	552.73	983.57	1073

Table S2. The intensity ratio of D/G peak according to Raman spectra of the PCE.

Laser Power (W)	9	12	15	18
D/G	1.039	0.862	1.052	1.012

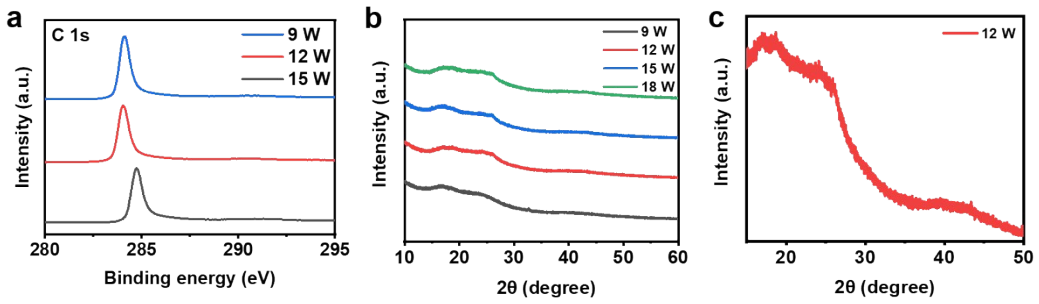

Figure S4. a) C 1s XPS spectra of PCE at different laser power. b) XRD spectra of PCE at different laser power. c) XRD spectra of PCE prepared with the laser power of 12 W

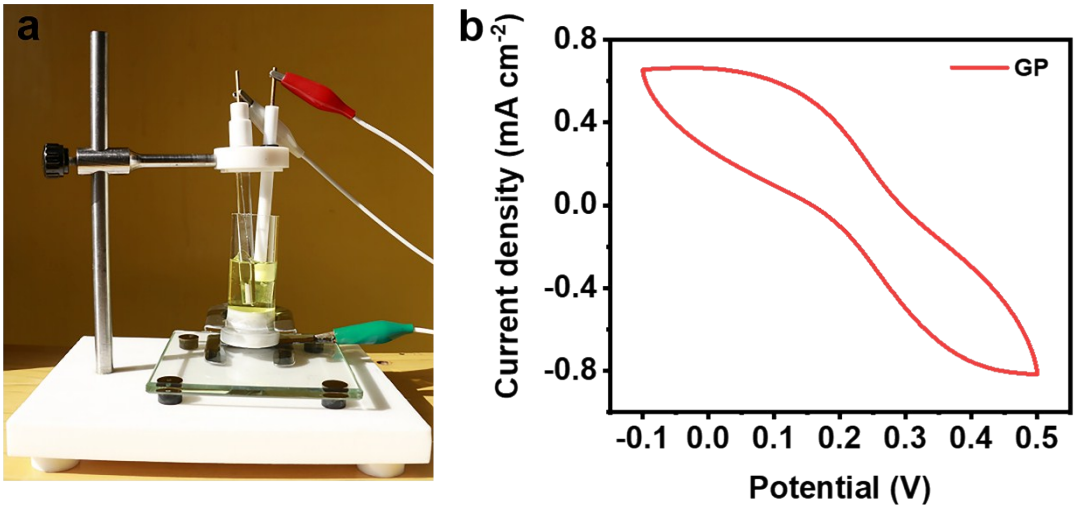

Figure S5. a) The set-up diagram for testing electrochemical properties. b) CV curve of GP substrate in the electrolyte solution (1 mM of potassium ferricyanide) at a scan rate of 50 mV s^{-1}.

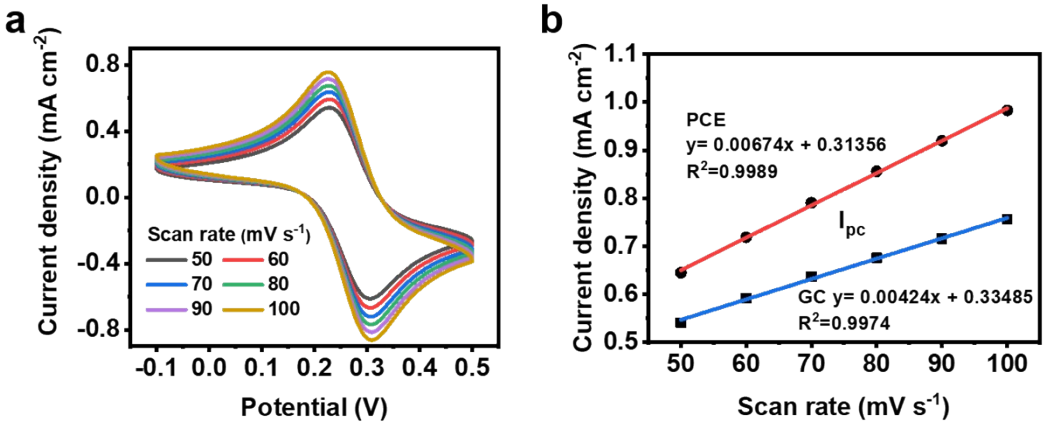

Figure S6. a) GC electrode at a scan rate from 50 to 100 mv s^{-1}.The CV curves are affected by the electrochemical scan rates in the electrolyte solution (1 mM potassium ferricyanide). b) The relationship between the scan rates and the cathode peak current densities of GC electrode and PCE.

Table S3. The prices of raw materials and GC electrode.

Material	Price ($)	Unit
Phenolic resin solution	13	L
Polyimide solution	135	L
Graphite paper (thickness is 1 mm)	9	m^2
Polyester fiber (thickness is 1 mm)	1	m^2
Glassy carbon electrode (diameter is 3 mm)	20	/

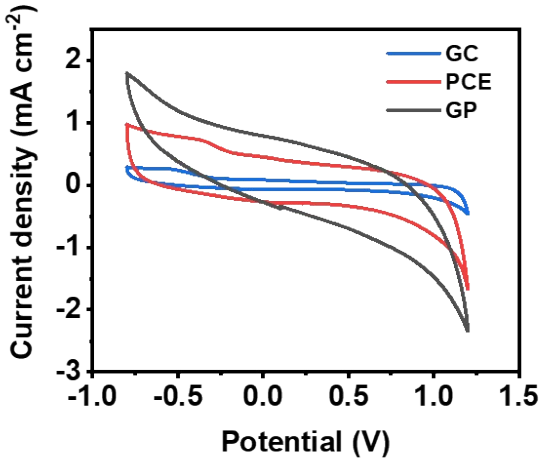

Figure S7. a) CV curves of GC, PCE and GP in 0.01 M PBS (PH=7.4).

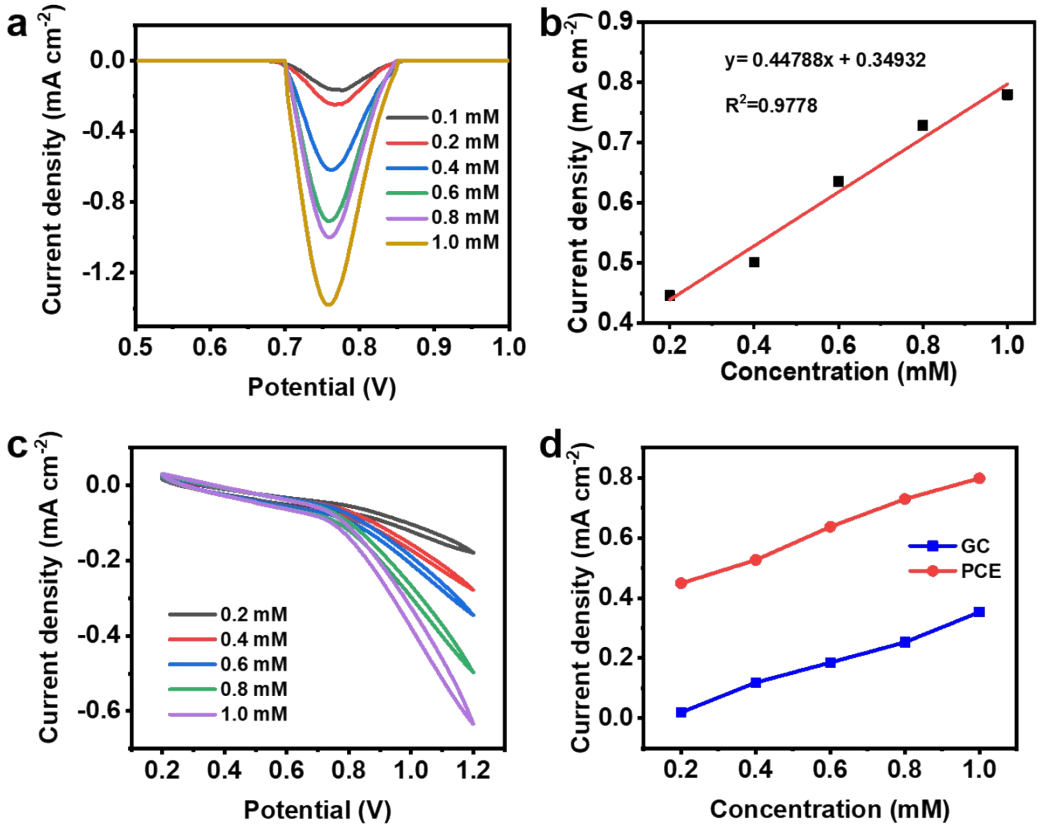

Figure S8. a) DPV curves of PCE with NTT in different concentrations. b) The relationship between the (-) anode peak current densities and the concentrations of NTT obtained from a). c) CV curves of GC with NTT in different concentrations. d) The anode peak current densities between the GC electrode and PCE in different concentrations of NTT solution.

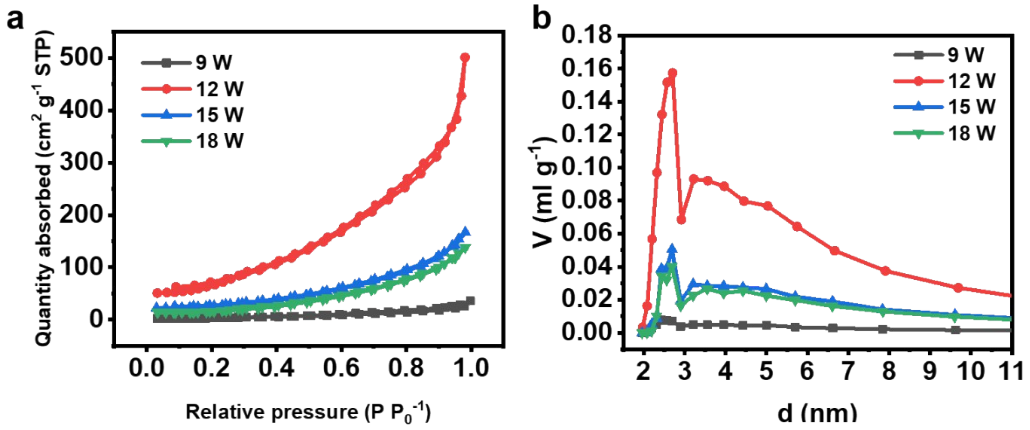

Figure S9. The BET data of PCE. a) N_2 adsorption-desorption isotherms of PCE prepared with different laser power. b) BJH pore size distributions of PCE.

Table S4. The BET data of PCE.

Laser power (W)	Specific surface ($m^2 g^{-1}$)	Pore diameter (nm)	Pore volume ($mL g^{-1}$)
9	14	15.66	0.0549

12	283	10.95	0.7751
15	99	10.46	0.2577
18	66	12.89	0.2133

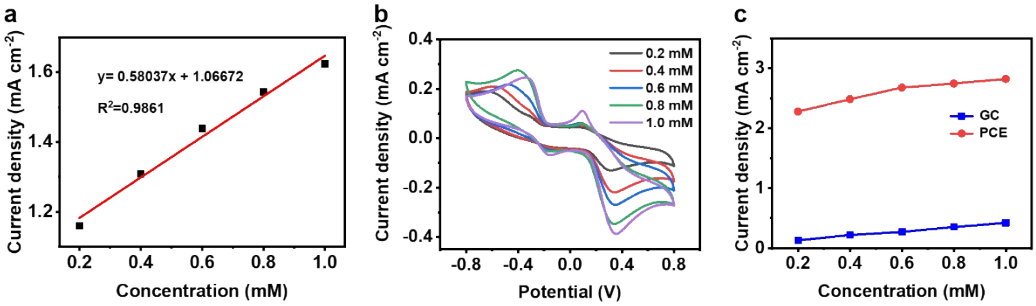

Figure S10. a) The relationship between the cathode peak current densities and the concentrations of DA obtained from Figure 2f. b) CV curves of GC with DA in different concentrations at a scan rate of 50 mV s^{-1}. c) The cathode peak current densities between the GC electrode and PCE in different concentrations of DA solution at a scan rate of 50 mV s^{-1}.

Table S5. Electrochemical parameters of PCE and the electrode materials of reported literature.

Electrode material	Electrolyte solution	Scan rate (mV s^{-1})	ΔE_p (mV)	I_{pa} (mA cm^{-2})	I_{pc} (mA cm^{-2})	Ref.
PCE	1 mM $[Fe(CN)_6]^{3-/4-}$	10	59	0.3575	0.3395	This work
LSG	1 mM $[Fe(CN)_6]^{3-/4-}$	10	59	0.0527	0.0541	1
Cu_2O-RGO-GCE	5 mM $[Fe(CN)_6]^{3-/4-}$	100	100	/	0.1171	2
Au-RGO-GCE	10 mM $[Fe(CN)_6]^{3-/4-}$	50	79	/	0.0159	3
PCE	0.1 mM NO_2^- in 0.01 M PBS	50	/	/	0.407	This work
GCE	0.1 mM NO_2^- in 0.01 M PBS	50	/	/	/	This work
Au-f-GE-GCE	5 mM NO_2^- in 0.1 M PBS	50	/	/	1.9226	4
ERHG-GCE	1 mM NO_2^- in 0.1 M PBS	50	/	/	0.495	5
GC-Au-MOF-5	1 mM NO_2^- in 0.1 M PBS	20	/	/	0.198	6

CuS-MWCNTs	4 mM NO_2^- in 0.1 M PBS	40	/	/	2.001	7
NGQDs@NCNFs-.GCE	1 mM NO_2^- in 0.1 M PBS	50	/	/	0.291	8
PCE	0.1 mM DA in 0.01 M PBS	50	/	2.2742	1.1350	This work
GCE	0.1 mM DA in 0.01 M PBS	50	/	0.0444	0.1297	This work
Bare-GCE	0.01 mM DA in 0.1 M PBS	100	/	0.0722	0.0519	2
Cu_2O-RGO-GCE	0.01 mM DA in 0.1 M PBS	100	/	0.6314	0.4603	2
Au-RGO-GCE	1 mM DA in 0.1 M PBS	50	/	0.02242	/	3

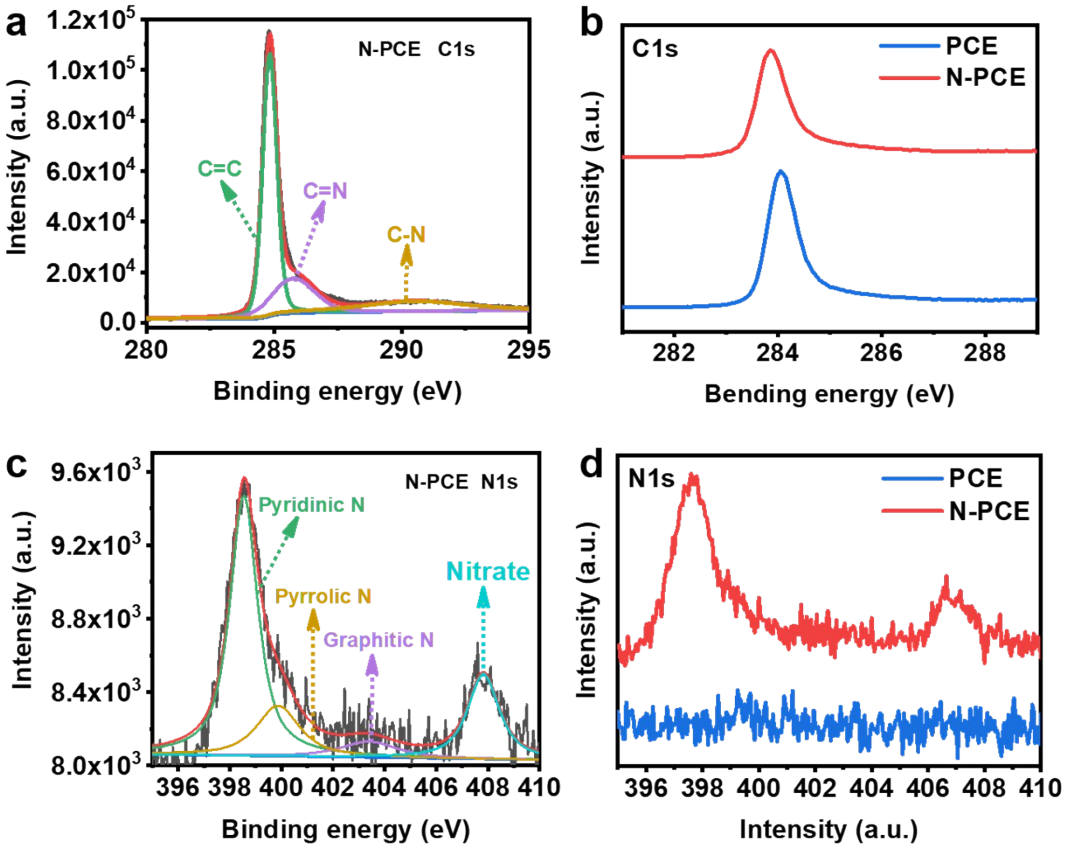

Figure S11. a) and b) C 1s XPS spectra of PCE and N-PCE. c) and d) N 1s XPS spectra of PCE and N-PCE.

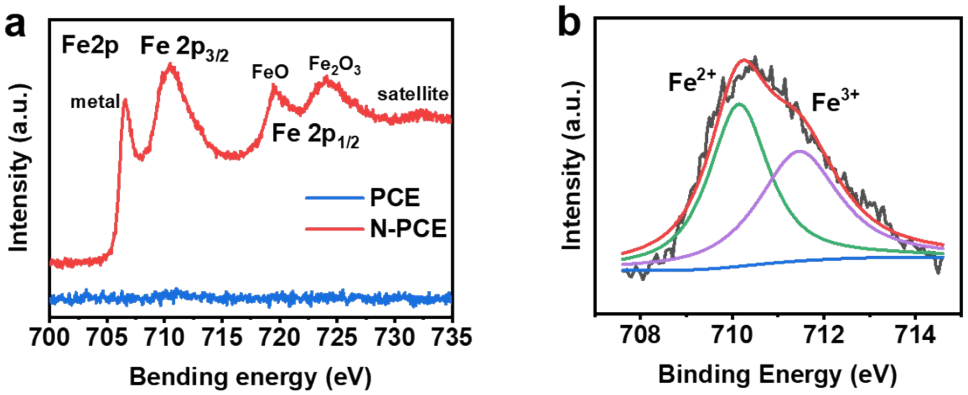

Figure S12. a) Fe 2p XPS spectra of PCE and N-PCE. b). Fe $2p_{3/2}$ XPS spectra of N-PCE.

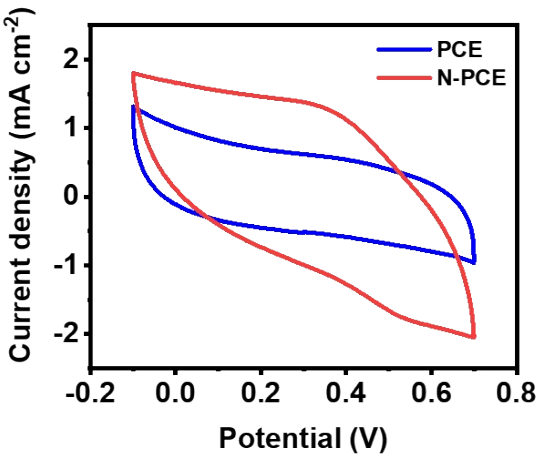

Figure S13. The CV curves of PCE and N-PCE in a 2 M H_2SO_4 electrolyte solution at a scan rate of 50 mV s^{-1}.

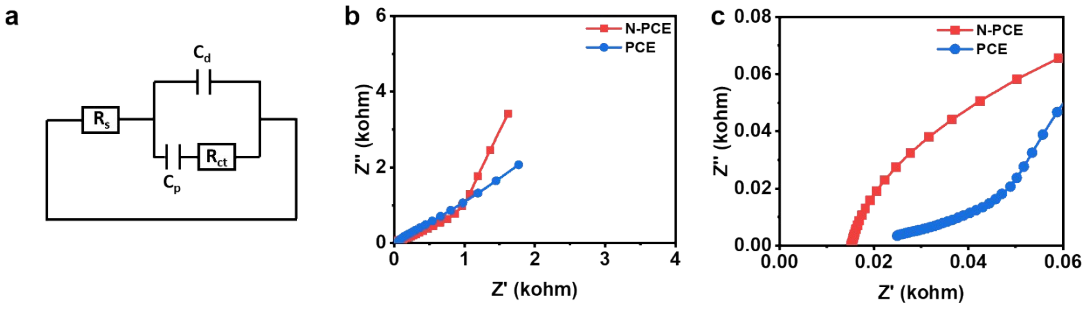

Figure S14. a) The equivalent circuit diagram. b) Nyquist curves of PCE and N-PCE in the range of 10 kHz to 10 MHz. c) The magnification for the high-frequency region.

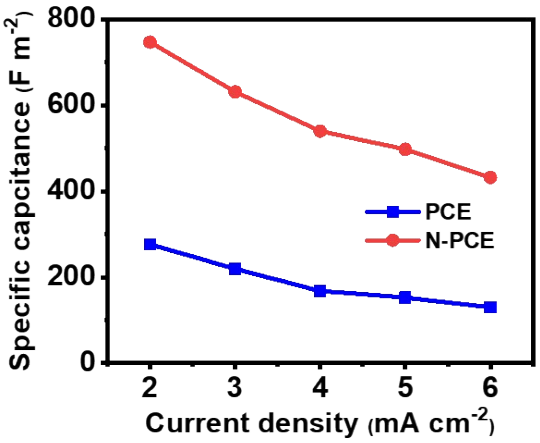

Figure S15. a) The specific capacitance of PCE and N-PCE at a current densities range of 2 and 6 mA cm^{-2}.

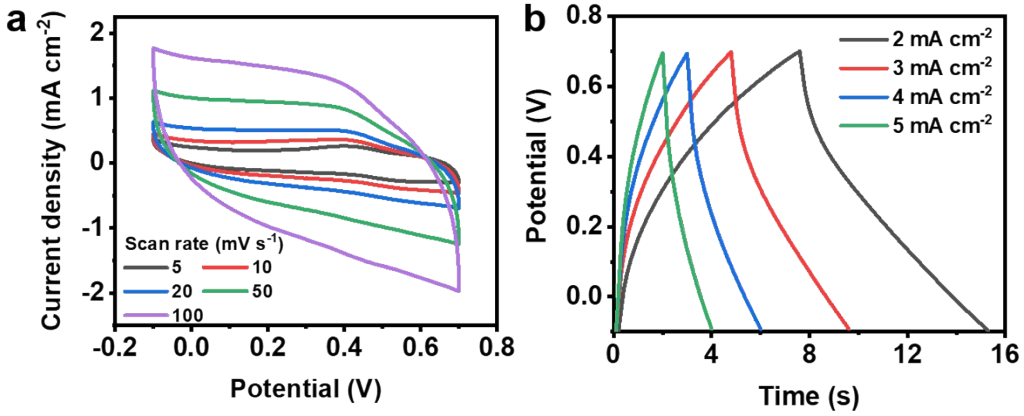

Figure S16. a) CV curves of N-PCE were affected by the electrochemical scan rates in a 2 M H_2SO_4 electrolyte solution. b) Galvanostatic charge-discharge curves of N-PCE (the amount of PB was 0.05 %) at different current densities in a 2 M H_2SO_4 electrolyte solution.

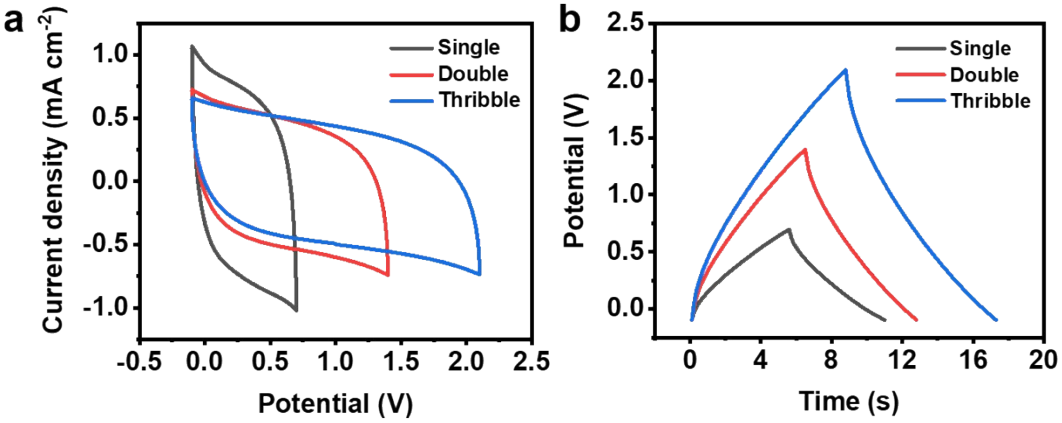

Figure S17. a) CV curves of N-PCE in single and series at a scan rate of 100 mV s^{-1}. b) Galvanostatic charge-discharge curves of N-PCE in single and series at a current density of 1 mA cm^{-2}.

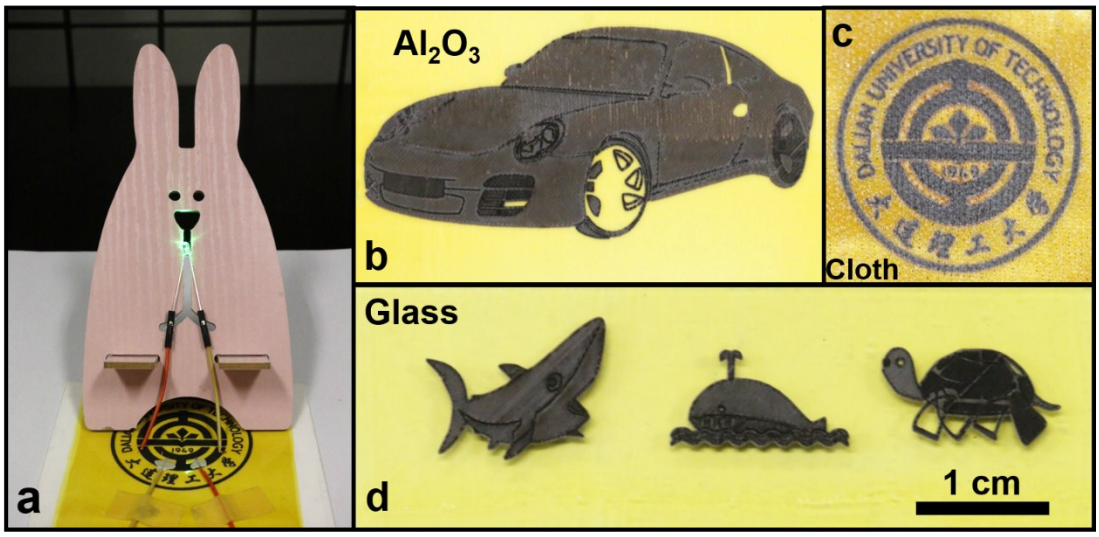

Figure S18. PR patterned on different substrates. a) A green LED was lighted by a DC power with conductive porous carbon material which was prepared on an aluminum oxide substrate. b) Aluminum oxide. c) Cloth. d) Glass.

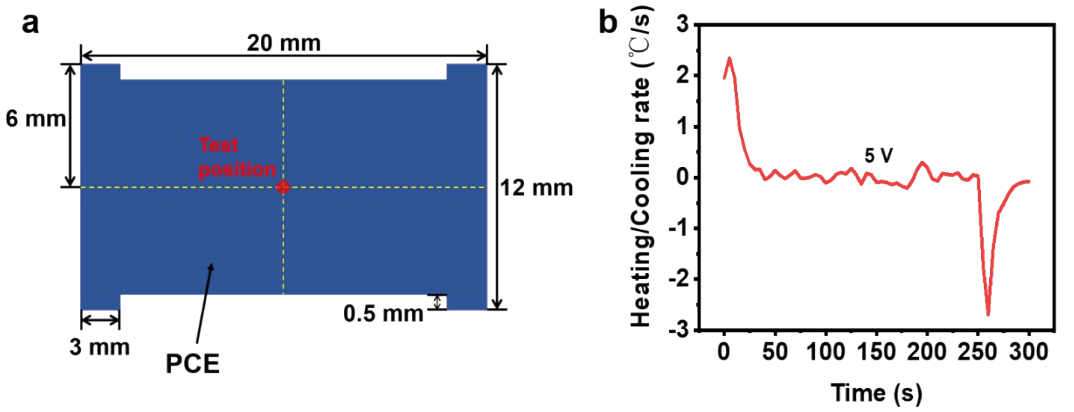

Figure S19. a) The illustration of the test position of the PCE heater. b) The curve of the derivative of the temperature to time at an applied voltage of 5 V for PCE heater.

Notes and references

1 K.Griffiths, C. Dale, J. Hedley, M. D. Kowal, R. B. Kaner and N. Keegan, *Nanoscale.*, 2014, **6**, 13613-13622.
2 Q. He, J. Liu, X. Liu, G. Li, P. Deng and J. Liang, *Sensors.*, 2018, **18**, 199.
3 C. Wang, D. Jiao, H. Wang, C. E. Zou, F. Jiang, Y. Ping and Y. Du, *Sens. Actuator B-Chem.,* 2014, **204**, 302-309.
4 C. Zou, B. Yang, D. Bin, J. Wang, S. Li, P. Yang, C. Wang, Y. Shiraishi and Y. Du, *J. Colloid. Interf. Sci.*, 2017, **488**, 135-141.
5 J. Zhang, Y. Zhang, J. Zhou and L. Wang, *Anal. Chim. Acta*., 2018, **1043**, 28-34.
6 D. K. Yadav, V. Ganesan, P. K. Sonkar, R. Gupta and P. K. Rastogi, *Electrochim. Acta.*, 2016, **200**, 276-282.
7 S. Zhang, B. Li, Q. Sheng and J. Zheng, *J. Electroanal. Chem.*, 2016, **769**, 118-123.
8 L. Li, L. Dong, K. Wang, H. Mao and T. You, *Sens. Actuator B-Chem.,* 2017, **252**, 17-23.